THE EUROPEAN
PHYSICAL JOURNAL C

Excess of tau events at SND@LHC, FASERν and FASERν2

Saeed Ansarifard[a] , **Yasaman Farzan**[b]

School of physics, Institute for Research in Fundamental Sciences (IPM), P.O. Box 19395-5531, Tehran, Iran

Abstract During the run III of the LHC, the forward experiments FASERν and SND@LHC will be able to detect the Charged Current (CC) interactions of the high energy neutrinos of all three flavors produced at the ATLAS Interaction Point (IP). This opportunity may unravel the mysteries of the third generation leptons. We build three models that can lead to a tau excess at these detectors through the following Lepton Flavor Violating (LFV) beyond Standard Model (SM) processes: (1) $\pi^+ \to \mu^+ \nu_\tau$; (2) $\pi^+ \to \mu^+ \bar{\nu}_\tau$ and (3) $\nu_e + \text{nucleus} \to \tau + X$. We comment on the possibility of solving the $(g-2)_\mu$ anomaly and the τ decay anomalies within these models. We study the potential of the forward experiments to discover the τ excess or to constrain these models in case of no excess. We then compare the reach of the forward experiments with that of the previous as well as next generation experiments such as DUNE. We also discuss how the upgrade of FASERν can distinguish between these models by studying the energy spectrum of the tau.

1 Introduction

Among the three neutrinos in nature, the tau-neutrino is the least studied one. Although the existence of ν_τ had been established by the precise measurement of the Z boson invisible decay width, its direct detection (i.e., detection of τ from the Charged Current (CC) interaction of ν_τ) was announced only in the early 21st century by the DONUT experiment at FermiLAB [1]. Indeed, the ν_τ data sample does not exceed ~ 21 events, consisting of the 9 DONUT events [2], the 10 ν_τ events registered by OPERA long baseline experiment [3] and two high energy cosmic ν_τ candidate events by ICE-CUBE [4]. The main reason why registering ν_τ events is so difficult is that the produced τ at low energies is too short-lived to lead to a discernible track. Moreover, the conven-

tional sources for neutrinos such as nuclear beta processes, muon decay or pion and Kaon decay produce only neutrinos of the first or second generations. The ν_τ detected by OPERA comes from the oscillation of ν_μ produced at CERN SPS en route to the detector at the Gran Sasso underground lab in Italy. Most likely, the high energy cosmic ν_τ flux is also produced from the oscillation of ν_μ and ν_e fluxes propagating from the source to the detector. At the DONUT experiment, however, the ν_τ flux was the decay product of heavy mesons.[1]

The FASERν [9] and SND@LHC [10,11] detectors during the run III of the LHC (2022-2024) will bring about a breakthrough in studying ν_τ. FASERν and SND@LHC are dense detectors, designed to detect (and distinguish) all three kinds of neutrinos. These experiments can also be sensitive to a variety of new physics involving dark matter [12–16] or beyond SM interaction of ν_μ [11,17–25].

In this paper, we explore three new scenarios that can lead to the overproduction of the τ events at forward experiments, FASERν and SND@LHC. We build models for these scenarios based on adding new scalar doublets to the SM. We show how by imposing global $U(1)$ flavor symmetries, the desired flavor structure of the Yukawa coupling can be obtained. As a bonus, these symmetries can explain the smallness of the first generation leptons and quarks. In each case, we show that how present experimental and observational constraints can be avoided and suggest strategies to test the accompanying prediction of the model by various experiments.

[a] e-mail: ansarifard@ipm.ir (corresponding author)

[b] e-mail: yasaman@theory.ipm.ac.ir

---

[1] We have to remind that more than 2 k atmospheric ν_τ event have been registered by super-Kamiokande and ICECUBE [5–8]. However, on an event by events basis, it is not possible to determine whether a given atmospheric neutrino event originates from a tau neutrino or not. Nevertheless, nonzero ν_τ component of the upward-going atmospheric neutrino flux (mainly originated from the oscillation of atmospheric ν_μ) has been established by both ICECUBE and super-Kamiokande [5–8]. Moreover, the average cross section of the charged current interaction of ν_τ has been measured by these experiments with a precision of $\sim 20\%$. Such precision is not enough to probe new physics, leading to per mill deviation from the SM prediction that we are here interested in.

The scenarios are the following: (1) $\pi^+ \rightarrow \mu^+ \nu_\tau$ with a branching ratio of $\sim 10^{-3}$. We show that this process can be obtained by adding scalar doublets to the SM such that their charged components are mixed. Despite the stringent bounds from the processes such as $\tau^+ \rightarrow \mu^+ \pi^0$, we show that within our model $Br(\pi^+ \rightarrow \mu^+ \nu_\tau) \sim 10^{-3}$ can be achieved. (2) $\pi^+ \rightarrow \mu^+ \bar{\nu}_\tau$ with again $Br(\pi^+ \rightarrow \mu^+ \bar{\nu}_\tau) \sim 10^{-3}$. The model that we build to embed this scenario involves a singlet charged scalar with an asymmetric coupling to the second and third generation of left-handed leptons. Such a coupling has been proposed in [26] to explain the anomalies observed in the tau decay. (3) τ production via ν_e (ν_μ) scattering off the matter fields. In the model that we build for this scenario, τ and ν_e (ν_μ) have a Yukawa coupling with a new scalar doublet. We discuss the present bounds from the NOMAD data on the cross section of this process and then derive improvements that can be brought about by the upcoming FASERν and SND@LHC experiments.

Ref. [22] discusses the bounds to be derived from FASERν on the effective couplings that can lead to processes $\pi^+ \rightarrow \mu^+ \nu_\tau$ and $\nu_e + \text{nucleus} \rightarrow \tau + X$. The bounds that we have found for FASERν are in good agreement with theirs. We proceed with deriving the shape of the spectrum of τ for each scenario and comparing with the background τ spectrum within the Standard Model. We show that studying the spectrum during the high luminosity phase of the LHC at FASERν 2 will dramatically increase the sensitivity to new physics. We also discuss the impact of the uncertainty in the prediction of the ν_τ flux within the Standard Model.

We show that the effects of $\pi^+ \rightarrow \mu^+ \bar{\nu}_\tau$ and the τ production by ν_e can be also described in terms of Charged Current (CC) Non-Standard Interaction (NSI) and the modified coherent source and detector eigenstates. In other words, we build viable models for sizable CC-NSI with observable effects at long baseline experiments such as DUNE.

This paper is organized as follows. In Sects. 2.1, 2.2 and 2.3, we describe the models that give rise to the τ excess at forward experiments as mentioned above. We outline the parameter ranges that lead to a sizable excess and discuss their predictions for the CMS and ATLAS, anomalous muon magnetic dipole moment and rare decays of the tau. In Sect. 2.4, we show how the effects predicted by these models can be described within the well-studied formalism of the Charged Current (CC) Non-Standard Interaction (NSI). We show that, thanks to a $m_\pi^2/(m_u + m_d)^2$ enhancement, we can obtain sizable CC NSI. We interpret the constraints on the CC NSI as bounds on our model. In Sect. 3, we derive the spectrum of τ within each model and discuss how the spectrum can help to discriminate between the Standard Model (SM) background for the τ events and the signals. In Sect. 4, we describe the relevant characteristics of the forward experiments of our interest and show that during the

run III, FASERν can significantly reduce the uncertainty in the SM prediction for the number of the τ events.

In Sect. 5, we discuss the signature of the models in the forward experiments and present our results for the upcoming SND@LHC and FASERν experiments as well as for the FASERν upgrade with higher statistics. A summary and discussion is given in Sect. 6.

2 The model(s)

In this section, we introduce the models for (i) $\pi^+ \rightarrow \mu^+ \nu_\tau$; (ii) $\pi^+ \rightarrow \mu^+ \bar{\nu}_\tau$ and (iii) the τ production by ν_e (ν_μ) scattering off the matter fields. In each case, we review the bounds on the parameter space of the model. As we shall discuss, in the lepton number violating model leading to $\pi^+ \rightarrow \mu^+ \bar{\nu}_\tau$, a Majorana neutrino mass of $O(10^{-3})$ eV is induced at the two-loop level which is too tiny to violate the upper bounds on neutrino mass. To explain the neutrino mass, the models should be extended to include a mechanism such as seesaw.

We then show how the effects of these new models in the neutrino experiments can be described by the coherent $|\nu^d\rangle$ and $|\nu^s\rangle$ states that have extensively been used in the literature to describe the CC-NSI.

2.1 A model for $\pi^+ \rightarrow \mu^+ \nu_\tau$

The $\pi^+ \rightarrow \mu^+ \nu_\tau$ process is constrained by the precision measurement of the ratio $Br(\pi \rightarrow e\nu)/Br(\pi \rightarrow \mu\nu)$ where ν can be any neutral fermion with a mass below 1 MeV that appears as missing energy. Notice that the SM prediction for this ratio is free from the uncertainties in the pion decay constant. The measurement is compatible with the SM prediction to the level of 2.4×10^{-3} [27], implying that $Br(\pi^+ \rightarrow e^+ \nu_\tau) < 2.4 \times 10^{-3} Br(\pi^+ \rightarrow e^+ \nu_e) = 2.8 \times 10^{-7}$ and $Br(\pi^+ \rightarrow \mu^+ \nu_\tau) < 2.4 \times 10^{-3} Br(\pi^+ \rightarrow \mu^+ \nu_\mu) = 2.4 \times 10^{-3}$.[2] Since the bound on $Br(\pi^+ \rightarrow e^+ \nu_\tau)$ is too strong to lead to an observable effect at FASERν and other similar experiments, we will only focus on $\pi^+ \rightarrow \mu^+ \nu_\tau$.

The effective four-Fermi coupling

$$G_{\nu\mu} \left(\bar{\mu} \frac{1 - \gamma_5}{2} \nu_\tau \right) \left(\bar{d} \frac{1 \pm \gamma_5}{2} u \right) \tag{1}$$

leads to

$$\Gamma(\pi^+ \rightarrow \mu^+ \nu_\tau) = G_{\nu\mu}^2 \frac{m_\pi}{32\pi} \frac{F_\pi^2}{(m_u + m_d)^2} (m_\pi^2 - m_\mu^2)^2. \tag{2}$$

---

[2] In this conclusion, we dismiss the accidental possibility that $Br(\pi^+ \rightarrow e^+ \nu_\tau)/Br(\pi^+ \rightarrow e^+ \nu_e) = Br(\pi^+ \rightarrow \mu^+ \nu_\tau)/Br(\pi^+ \rightarrow \mu^+ \nu_\mu)$. If this equality holds, the constraint on $Br(\pi \rightarrow e\nu)/Br(\pi \rightarrow \mu\nu)$ does not constrain $Br(\pi^+ \rightarrow \mu^+ \nu_\tau)$ or $Br(\pi^+ \rightarrow e^+ \nu_\tau)$, separately.

Table 1 The $U_1(1) \times U_2(1)$ charges of the fields. The rest of the fields, including u_R and the Higgs are taken neutral under $U_1(1) \times U_2(1)$

Charges	Φ_1	Φ_2	L_τ, τ_R	L_μ, μ_R	Q	d_R
$U_1(1)$	1	0	0	0	β	$\beta - 1$
$U_2(1)$	0	1	α	$1 + \alpha$	0	0

With $G_{\nu\mu} \sim 4 \times 10^{-8}$ GeV^{-2}, $Br(\pi^+ \to \mu^+ \nu_\tau) \sim 10^{-3}$. Notice that although the $G_{\nu\mu}$ coupling is chirality-flipping, the angular momentum conservation and the fact that both interactions are short-ranged imply that the polarizations of the muons emitted in $\pi^+ \to \mu^+ \nu_\tau$ and $\pi^+ \to \mu^+ \nu_\mu$ are equal. As a result, the precise measurement of the muon polarization [28] does not constrain $G_{\nu\mu}$.

To obtain the effective coupling in Eq. (1), we introduce two scalar doublets, $\Phi_1 = (\phi_1^+ \ \phi_1^0)^T$ and $\Phi_2 = (\phi_2^+ \ \phi_2^0)^T$ with the following Yukawa couplings with the doublets, $L_\tau = (\nu_\tau \ \tau_L)^T$ and $Q_1 = (u_L \ d_L)^T$:

$$\lambda_d \bar{d} \Phi_1^\dagger Q_1 + \lambda_u \bar{u} \Phi_1^T c Q_1 + \lambda_\mu \bar{\mu} \Phi_2^\dagger L_\tau + \text{H.c.,} \tag{3}$$

where c is an asymmetric matrix with $c_{12} = -c_{21} = 1$. If Φ_1 is identified with Φ_2 or if the neutral components of these two doublets are mixed, the effective LFV $G_\pi (\bar{\mu}_R \tau_L)(\bar{u}\gamma_5 u - \bar{d}\gamma_5 d)$ and $G_\eta (\bar{\mu}_R \tau_L)(\bar{u}\gamma_5 u + \bar{d}\gamma_5 d)$ couplings can be obtained by integrating out the heavy states. G_η and G_π will be respectively proportional to $\lambda_u + \lambda_d$ and $\lambda_u - \lambda_d$. These effective couplings lead to $\tau \to \mu\pi^0$ and $\tau \to \mu\eta^0$ which are severely constrained [28] and set bounds: $G_\pi < 5 \times 10^{-9}$ GeV^{-2} and $G_\eta < 4 \times 10^{-10}$ GeV^{-2}. To obtain $Br(\pi^+ \to \mu^+ \nu_\tau) \sim 10^{-3}$, we therefore need $G_{\nu\mu} \gg G_\pi, G_\eta$. This in turn implies $\Phi_1 \neq \Phi_2$. Moreover, the mixing between the neutral components of Φ_1 and Φ_2 should be much smaller than that between their charged components.[3]

To explain the flavor structure of the Yukawa couplings and to simplify the Lagrangian by removing unwanted terms, we impose an approximate $U_1(1) \times U_2(1)$ global symmetry. The $U_1(1) \times U_2(1)$ charges of the relevant fields are shown in Table 1. The rest of the SM fields are neutral under this new $U_1(1) \times U_2(1)$.

With this assignment, $\lambda_d \neq 0$ but $\lambda_u = 0$ so our analysis will be simplified. Notice that the Yukawa couplings of u and d to the SM Higgs breaks the $U_1(1)$ symmetry so the smallness of the u and d masses can be explained as a bonus in this model. We can proceed with assigning unequal $U_1(1) \times U_2(1)$ charges to e_R and L_e to also explain the lightness of the first generation of leptons but this is not the main goal of the present paper. The $U_1(1) \times U_2(1)$ symmetry explains the

flavor structure of the Yukawa couplings and forbids mixing terms between Φ_1 and Φ_2 such as $\Phi_1^\dagger \Phi_2$, $|H|^2 \Phi_1^\dagger \Phi_2$ and $(H^\dagger \Phi_1)(\Phi_2^\dagger H)$. As a result, ϕ_1^0 and ϕ_2^0 will not be mixed, preventing $\tau \to \mu\pi^0$.

The mixing between ϕ_1^+ and ϕ_2^+, which is required to obtain $\pi^+ \to \mu^+ \nu_\tau$, breaks $U_1(1) \times U_2(1)$. After electroweak symmetry breaking, we can obtain such a mixing between the charged components of Φ_1 and Φ_2 without mixing their neutral components via the following term

$$\lambda_{12}(H^T c \Phi_1)(\Phi_2^\dagger c H^*). \tag{4}$$

Notice that this term explicitly breaks the global $U_1(1) \times U_2(1)$ to a single $U(1)$ under which Φ_1 and Φ_2 have equal charges. The effective coupling $G_{\nu\mu}$ can be written as

$$G_{\nu\mu} = \frac{\lambda_\mu \lambda_d}{m_{\phi_1^+}^2} \frac{\lambda_{12} v^2 / 2}{m_{\phi_2^+}^2}$$
$$= 4 \times 10^{-8} \text{ GeV}^{-2} \frac{\lambda_\mu}{0.3} \frac{\lambda_d}{0.3} \frac{\lambda_{12}}{0.12} \frac{(300 \text{ GeV})^2}{m_{\phi_1^+}^2} \frac{(300 \text{ GeV})^2}{m_{\phi_2^+}^2}. \tag{5}$$

The λ_μ coupling can also give a contribution to $(g-2)_\mu$ of $\Delta a_\mu \sim \lambda_\mu^2 m_\mu^2 / (100\pi^2 m_{\Phi_2}^2)$ [29–32]. In order to account for the $(g-2)_\mu$ anomaly [33–38] with $m_{\Phi_2} \sim 300$ GeV, λ_μ should saturate the perturbativity bound: $\lambda_\mu \sim 3$. In fact, this is a general feature of the models that explain the $(g-2)_\mu$ anomaly with new Yukawa coupling [39]. To maintain $G_{\nu\mu} \sim 4 \times 10^{-8}$ GeV^{-2}, we can decrease λ_{12} by one order of magnitude. The smallness of λ_{12} can be explained by $U_1(1) \times U_2(1) \to U(1)$.

The components of Φ_2 can be pair produced at the LHC via the electroweak interactions. They will subsequently decay as $\phi_2^0 \to \mu^+ \tau^-$ and $\phi_2^+ \to \mu^+ \nu_\tau$. The components of Φ_1 can also be pair produced via the electroweak interactions. Moreover, the $\bar{d} + u$ and $\bar{d} + d$ scatterings can respectively produce ϕ_1^+ and ϕ_1^0 in association with the gluon. The Φ_1 components will subsequently decay into a pair of jets. Through the mixing between Φ_1 and Φ_2, the electroweak interaction can also produce $\Phi_1 \Phi_2$ pairs. Moreover, the mixing can lead to the leptonic (hadronic) decay modes for Φ_1 (Φ_2). These effects are however subdominant and further suppressed by $O[(\lambda_{12} v^2 / m_{\Phi_{1,2}}^2)^2]$. The heavier component of Φ_1 or Φ_2 can also decay into the lighter one and the W boson. The splittings between the two components are however constrained by the oblique parameters [40]. The signature of

---

[3] Notice that the mixing between the charged components can lead to a mixing between the neutral components at one loop, suppressed by $e^2 \sin^2 \theta_W / 16\pi^2 \sim 10^{-2}$ which is small enough.

pair production of the Φ_1 as well as single Φ_1 production in association of gluon(s) will be multijet signal which suffers from high background. To our best knowledge, ϕ_1 heavier than 200 GeV decaying into jets is still unconstrained by the LHC. However, it may be discovered during the high luminosity phase of the LHC. The signatures of the $\phi_2^+(\phi_2^0)^\dagger$, $\phi_2^-\phi_2^0$, $\phi_2^+\phi_2^-$ and $(\phi_2^0)^\dagger\phi_2^0$ are respectively $\mu^+\nu_\tau\mu^-\tau^+$, $\mu^-\bar{\nu}_\tau\mu^+\tau^-$, $\mu^+\nu_\tau\mu^-\bar{\nu}_\tau$ and $\mu^-\tau^+\mu^+\tau^-$ where the invariant masses of the τ and μ pairs are equal to $m_{\phi_2^0}$. To our best knowledge, neither a dedicated search for ϕ_2^0 with an arbitrary mass decaying into $\mu^+\tau^-$ nor a search for ϕ_2^+ decaying into the muon plus missing energy has been carried out, yet.[4]

Notice that $\pi^+ \to \mu^+\nu_\tau$ is enhanced by $f_\pi^2/(m_u + m_d)^2$ but the cross section of the ν_τ interaction on the nuclei via the new $G_{\nu\mu}$ does not enjoy such as enhancement. Moreover, since there is a large background for the (μ+jets) signal from the CC interaction of ν_μ, we do not need to worry about the impact of $G_{\nu\mu}$ on the detection.

In Sect. 5, we shall study the bounds from FASERν on $Br(\pi^+ \to \mu^+\nu_\tau)$. This scenario could lead to the tau production at the NOMAD detector, too. However, at NOMAD the energies of neutrinos from the pion decay are around 20 GeV so the momentum of the jets recoiling against the produced τ would be too low to survive the cuts applied by the NOMAD collaboration to identify the τ production [42]. At NOMAD, the neutrino flux with energies higher than 50 GeV was also produced but the production was dominated by the Kaon decay rather than the pion decay. As a result, the exotic decay $K^+ \to \mu^+\nu_\tau$ can already strongly be constrained by NOMAD. We have therefore focused only on the exotic pion decay in this paper.

2.2 A model for $\pi^+ \to \bar{\nu}_\tau\mu^+$ with a connection to observed anomalies in τ decay

Ref. [26] proposes a model to address the 2σ discrepancy between the observation and the SM prediction in the $\tau \to \mu\nu_\tau\bar{\nu}_\mu$ mode [43]. The model is based on the introduction of a new charged singlet Φ^+ heavier than 300 GeV and with an interaction of form

$$\mathscr{L} = -\frac{\lambda_{23}}{2}L_{a,\mu}\varepsilon_{ab}L_{b\tau}\Phi^+ + \text{H.c}$$
$$= -\frac{\lambda_{23}}{2}(\nu_\mu^T c\tau_L - \mu_L^T c\nu_\tau)\Phi^+ + \text{H.c} \quad (6)$$

From $\text{Br}(\tau \to \mu\nu\nu)/\text{Br}(\tau(\mu) \to e\nu\nu)$, Ref. [26] finds

$$0.052\frac{m_{\Phi^+}}{300\text{ GeV}} < \lambda_{23} < 0.148\frac{m_{\Phi^+}}{300\text{ GeV}}. \quad (7)$$

The λ_{23} coupling can also give rise to $(g-2)_\mu$ but considering the upper bound on λ_{23} shown in Eq. (7), the contribution will be too small to account for the observed deviation from the standard model prediction [29–34].

Let us reintroduce Φ_1 of Sect. 2.1 to this section with the $U(1)$ charges as in Table 2. With this assignment, we can have a trilinear term as

$$A\Phi^-H^Tc\Phi_1$$

which after electroweak symmetry breaking induces a mixing between Φ^+ and ϕ_1^+ given by

$$\sin 2\theta = \frac{2A\,v/\sqrt{2}}{m_{\phi_1^+}^2 - m_{\Phi^+}^2}. \quad (8)$$

Integrating out the heavy fields, we shall have an effective coupling of form

$$G_{\bar{\nu}\mu}\left(\bar{d}\frac{1-\gamma_5}{2}u\right)(\nu_\mu^Tc\tau_L - \mu_L^Tc\nu_\tau) + \text{H.c.} \quad (9)$$

where

$$G_{\bar{\nu}\mu} = \frac{\lambda_d\lambda_{23}}{2}\frac{Av/\sqrt{2}}{m_{\Phi^+}^2 m_{\phi_1^+}^2}.$$

With this effective Lagrangian, a new decay mode $\pi^+ \to \bar{\nu}_\tau\mu^+$ will open with a rate given by Eq. (2) but replacing $G_{\nu\mu}$ with $G_{\bar{\nu}\mu}$. Similarly to the decay via $G_{\nu\mu}$, with $G_{\bar{\nu}\mu} \sim 5 \times 10^{-8}$ GeV^{-2}, $\text{Br}(\pi^+ \to \bar{\nu}_\tau\mu^+)$ can be as large as 10^{-3}.

The axial component of $G_{\bar{\nu}\mu}$ can lead to

$$\Gamma(\tau^- \to \bar{\nu}_\mu\pi^-) \sim \frac{G_{\bar{\nu}\mu}^2}{4\pi}\frac{F_\pi^2m_\pi^2}{(m_u+m_d)^2}m_\tau \quad (10)$$

which is again enhanced by $m_\pi^2/(m_u + m_d)^2$. The corresponding branching ratio is $\text{Br}(\tau^- \to \bar{\nu}_\mu\pi^-) \sim 5 \times 10^{-6}[G_{\bar{\nu}\mu}/(5 \times 10^{-8}\text{ GeV}^{-2})]^2$ which is much smaller than the uncertainty in $\text{Br}(\tau \to \pi\nu)$ which is 5×10^{-4} [28]. Within the SM, the branching ratio of $\tau^- \to \nu_\tau\pi^0\pi^-$ is even larger than that of the two body decay $\tau^- \to \nu_\tau\pi^-$. The enhancement is due to the spin 1 ρ resonance from the vectorial part of the charged current, $\tau^- \to \nu_\tau\rho^- \to \nu_\tau\pi^0\pi^-$ [44,45]. In our model, since the mediator (Φ^+) has zero spin, no ρ resonance occurs so we expect $\tau^- \to \bar{\nu}_\mu\pi^0\pi^-$ to be suppressed. Via the $G_{\bar{\nu}\mu}$ interaction, ν_μ can produce τ in the detector, too, but the cross section will be suppressed by $\sim G_{\bar{\nu}\mu}^2/(8G_F^2) \sim 2 \times 10^{-6}$ relative to the SM CC interaction of ν_μ. This means the number of τ events produced

---

[4] There is already a stringent bound on the LFV decay mode of the SM Higgs: $Br(H \to \tau\mu) < 0.28\%$ [41]. This bound can be translated into an upper bound on the mixing between H^0 and ϕ_1^0. Such a mixing violates the global $U_1(1) \times U_2(1)$ symmetry as well as the residue $U(1)$ that survives the introduction of λ_{12}. Thus, in our model, the mixing between H^0 and ϕ_1^0 is naturally small.

Table 2 The $U(1)$ charges of the fields. The rest of the fields, including u_R and the Higgs are neutral under $U(1)$

Charges	Φ_1	Φ^+	L_τ, τ_R	L_μ, μ_R	Q	d_R
$U(1)$	1	1	$-1/2 - \alpha$	$-1/2 + \alpha$	β	$\beta - 1$

during the run III of the LHC by the ν_μ flux will be as small as $O(0.01)$ and therefore negligible. Similarly, the bound on the τ production at NOMAD [42] can be avoided.

In this model, Φ^+ and Φ^- can be pair produced at the HL-LHC by electromagnetic interactions. They will then decay as $\Phi^+ \to \mu^+ \nu$ and $\Phi^+ \to \tau^+ \nu$ so the signals will be excess in the $\mu^+ \mu^-$ + missing energy, $\tau^+ \tau^-$ + missing energy, $\tau^- \mu^+$ +missing energy and $\tau^+ \mu^-$ +missing energy signals. The Φ_1 pairs can also be produced at the LHC, decaying into jets as described in the previous subsection.

Since in this model, lepton number is violated, neutrinos can obtain a Majorana mass term. Notice that lepton number violation requires both the λ_{23} coupling and the mixing between Φ^+ and Φ_1^+. As a result, the neutrino mass generation in this model starts at two-loop level, inducing a mass of form $\nu_\tau^T c \nu_\mu$ of order of

$$G_{\bar{\nu}\mu} G_F (m_\tau^2 - m_\mu^2) \frac{(m_u + m_d)m_W^2}{(16\pi^2)^2} \sim \text{m}e\text{V}.$$

The $(m_\tau^2 - m_\mu^2)$ comes from a cancellation between the two diagrams in which μ and τ propagate. The induced mass is too small to violate the current upper bounds on the neutrino mass.

2.3 Non-standard τ production at the detector

In this section, we introduce a variation of the model introduced in Sect. 2.1 with the difference that Φ_2 couples to τ_R instead of μ_R as follows

$$\lambda_e \bar{\tau}_R \Phi_2^\dagger L_e + \lambda_\mu \bar{\tau}_R \Phi_2^\dagger L_\mu. \tag{11}$$

If λ_e and λ_μ are both nonzero, they can contribute to $\mu \to e\gamma$ at one loop which is severely constrained by the experimental bounds. As a result, we assume that only one of λ_e and λ_μ is nonzero. This pattern can be explained by the $U_2(1)$ symmetry. For example, if we assign $U_2(1)$ charges to Φ_2 and leptons as shown in Table 3, we can simultaneously explain nonzero λ_e, vanishing λ_μ and the smallness of the electron mass.

Like the model in Sect. 2.1, we allow only the charged components to mix with each other. As a result, the severely constrained decay modes $\tau^- \to e^- \pi^0$ or $\tau^- \to \mu^- \pi^0$ cannot be obtained at the tree level. However, we obtain

$$G_e(\bar{\tau}_R \nu_e)(\bar{u}_L d_R) \quad \text{or} \quad G_\mu(\bar{\tau}_R \nu_\mu)(\bar{u}_L d_R) \tag{12}$$

where $G_e = \lambda_d \lambda_e \lambda_{12} v^2 / (2m_{\phi_1^+}^2 m_{\phi_2^+}^2)$ and $G_\mu = \lambda_d \lambda_\mu \lambda_{12} v^2 / (2m_{\phi_1^+}^2 m_{\phi_2^+}^2)$. These effective couplings respectively lead to $\tau^- \to \pi^- + \nu_e$ and $\tau^- \to \pi^- + \nu_\mu$. Similarly to Sect. 2.1 and the case of $G_{\bar{\nu}\mu}$ in Eq. (10), the uncertainty on $\tau^+ \to \pi^+ \nu$ gives the constraint $G_{e(\mu)} < 5 \times 10^{-7} \text{ GeV}^{-2}$.[5] Saturating this constraint, we shall have $\sigma(\nu_{e(\mu)} + \text{nucleus} \to \tau + X)/\sigma(\nu_\mu + \text{nucleus} \to \mu + X) \sim (G_{e(\mu)}/4G_F)^2 \sim 10^{-4}$. In this model, regardless of the origin of the neutrinos (whether they come from the pion or Kaon decays), the electron or muon neutrinos with energies sufficiently larger than the tau mass can lead to the production of τ. As a result, the NOMAD experiment can constrain G_e and G_μ (cf. the model in Sect. 2.1 which avoids the NOMAD constraints as explained.) The number of the ν_μ charged current events with an energy larger than 25 GeV observed at NOMAD was above 2×10^5 which is one order of magnitude larger than the anticipated number at FASERν during run III. The bound from NOMAD on G_μ would therefore be of order of $5 \times 10^{-8} \text{ GeV}^{-2}$ which is even stronger than the bound from $\tau^+ \to \pi^+ \nu_\mu$. Such a strong bound on G_μ makes observing a deviation from the SM prediction at FASERν hopeless so we shall not study the effects of G_μ at FASERν any further. On the other hand, the number of the ν_e events at NOMAD and FASERν are comparable so the bound on G_e may be improved by FASERν. In Sect. 2.4, we will quantify the bound from NOMAD on G_e. We shall study the bound that FASERν and its upgrades can set on $\sigma(\nu_e + \text{nucleus} \to \tau + X)$ in Sect. 6.

2.4 Connection to the charged current non-standard interaction formalism

There is a rich literature studying the Non-Standard Interaction (NSI) on neutrino oscillation experiments [46]. The effects of Charged Current NSI are often analyzed by introducing eigenstates of source and detector as follows

$$|\nu_\alpha^s\rangle = |\nu_\alpha\rangle + \sum_{\gamma \in \{e, \mu, \tau\}} \varepsilon_{\alpha\gamma}^s |\nu_\gamma\rangle \tag{13}$$

---

[5] Notice that the bound that we have found on G_e from $\tau^+ \to \pi^+ \nu_e$ is much stronger than the bound in [22]. To derive this bound we have equated $Br(\tau^+ \to \pi^+ \nu_e)$ with the experimental uncertainty in $Br(\tau^+ \to \pi^+ + \nu)$ which is 5×10^{-4}.

Table 3 The $U_2(1)$ charges of the fields. The rest of the fields, including the second generation leptons, Φ_1, quarks and the Higgs are neutral under $U_2(1)$

Charges	Φ_2	L_τ, τ_R	L_e	e_R, H, quarks, L_μ, μ_R, Φ_1
$U_2(1)$	1	b	1+b	0

and

$$\langle \nu_\alpha^d | = \langle \nu_\alpha | + \sum_{\gamma \in \{e,\mu,\tau\}} \varepsilon_{\gamma\alpha}^d \langle \nu_\gamma | \qquad (14)$$

where $|\nu_\alpha^s\rangle$ is the eigenstate produced in the source along with the charged lepton of flavor α and $|\nu_\alpha^d\rangle$ is the eigenstate which can produce the charged lepton of flavor α in the detector. Within the SM, $|\nu_\alpha^s\rangle = |\nu_\alpha^d\rangle = |\nu_\alpha\rangle$. However, non-standard interaction can in principle induce nonzero $\varepsilon_{\alpha\beta}^s$ and $\varepsilon_{\alpha\beta}^d$. In recent years, a class of models have been developed based on a new light neutral $U(1)$ gauge boson coupled to neutrinos and matter fields that induces a sizable neutral current NSI [47–51]. In case of CC NSI, the mediator has to be a charged particle so its mass must be heavier than a few 100 GeV to avoid direct production at the LEP and/or at the LHC. Since the relevant effective four-Fermi coupling is given by inverse of the square of the mediator mass, a strong lower bound on the mediator mass generally means small CC NSI. With this consideration, not many models are proposed to underly the CC NSI, despite the extensive efforts to study their phenomenological impact on the neutrino experiments. Indeed, $G_{\nu\mu}$ obtained in Eq. (5) is quite suppressed $G_{\nu\mu} \ll G_F$. Despite the smallness of $G_{\nu\mu}$, thanks to the $m_\pi/(m_u + m_d)$ enhancement in the amplitude of $\pi^+ \to \mu^+\nu_\tau$ relative to that of the standard $\pi^+ \to \mu^+\nu_\mu$, $Br(\pi^+ \to \mu^+\nu_\tau)$ can be still relatively large. Within the model introduced in Sect. 2.1, $|\nu_\mu^s\rangle$ can be written as

$$|\nu_\mu^s\rangle = \frac{\mathscr{M}_1|\nu_\mu\rangle + \mathscr{M}_2|\nu_\tau\rangle}{\sqrt{|\mathscr{M}_1|^2 + |\mathscr{M}_2|^2}} \simeq |\nu_\mu\rangle + \mathscr{M}_2/\mathscr{M}_1|\nu_\tau\rangle, \qquad (15)$$

where $\mathscr{M}_1$ and $\mathscr{M}_2$ are respectively the amplitudes of $\pi^+ \to \mu^+\nu_\mu$ and $\pi^+ \to \mu^+\nu_\tau$. Thus, in the model introduced in Sect. 2.1,

$$\varepsilon_{\mu\tau}^s = \frac{\mathscr{M}_2}{\mathscr{M}_1}.$$

We can therefore write $|\varepsilon_{\mu\tau}^s|^2 = |\mathscr{M}_2|^2/|\mathscr{M}_1|^2 \simeq Br(\pi^+ \to \mu^+\nu_\tau)$. In this model, $\varepsilon_{\mu\tau}^d \ll 1$. If the baseline of the experiment is short such that $\Delta m_{atm}^2 L/E_\nu \ll 1$, the number of the μ events and the excess of the τ events in the detector will respectively be given by $Br(\pi^+ \to \mu^+\nu_\mu)\sigma_{SM}(\nu_\mu \to \mu)$ and $Br(\pi^+ \to \mu^+\nu_\tau)\sigma_{SM}(\nu_\tau \to \tau)$. Thus, it is valid to analyze the FASERν results as well as the DUNE near detector data in terms of $Br(\pi^+ \to \mu^+\nu_\tau)$ rather than studying the

evolution of the coherent state in Eq. (15). However, for the long baseline experiments, it is necessary to study the evolution of the full coherent state in Eq. (15); otherwise, we will miss the effect of the interference terms given by

$$2Re[U_{\mu i}U_{\mu i}^* U_{\mu j}^* U_{\tau j}(\varepsilon_{\mu\tau}^s)^* e^{i(m_i^2 - m_j^2)L/(2E_\nu)}]$$

in case of the μ detection and

$$2Re[U_{\tau i}U_{\mu i}^* U_{\tau j}^* U_{\tau j}(\varepsilon_{\mu\tau}^s)^* e^{i(m_i^2 - m_j^2)L/(2E_\nu)}]$$

in case of the τ detection. Notice that both these interference terms are linear in $\varepsilon_{\mu\tau}^s$ and therefore dominate over the effect of $Br(\pi^+ \to \mu^+\nu_\tau) = |\varepsilon_{\mu\tau}^s|^2$.

In case of $\nu_{e(\mu)}$ + nucleus $\to \tau + X$ within the model introduced in Sect. 2.3, we should pay attention that the chirality of τ produced via the new coupling is opposite to that produced by ν_τ in the SM. As a result, the interference term will be suppressed by m_τ/E_ν and we cannot therefore simply equate $\varepsilon_{e(\mu)\tau}^d$ with $\mathscr{M}(\nu_{e(\mu)} + \text{nucleus} \to \tau + X)/\mathscr{M}(\nu_\tau + \text{nucleus} \to \tau + X)$. In fact, the helicity of the final τ has to be considered, too. For short baseline experiment such as FASERν or NOMAD for which $\Delta m_{atm}^2 L/(2E_\nu) \ll 1$, such interference is not relevant and we can use the bounds on $\varepsilon_{e(\mu)\tau}^d$ and on $[\sigma(\nu_{e(\mu)} + \text{nucleus} \to \tau + X)/\sigma(\nu_\tau + \text{nucleus} \to \tau + X)]^{1/2} \simeq G_{e(\mu)}/(\sqrt{96}G_F)$, interchangeably. As discussed in Sect. 2.3, the NOMAD experiment can constrain this model. From the NOMAD data, Ref. [52] finds $\varepsilon_{e\tau}^d < 0.087$ which implies $\sigma(\nu_{e(\mu)} + \text{nucleus} \to \tau + X)/\sigma(\nu_\tau + \text{nucleus} \to \tau + \text{nucleus}) < 0.0075$ and $G_{e(\mu)}/G_F < 0.85$ which is readily satisfied in the model described in Sect. 2.3.

The far detector of DUNE can also constrain ε^d and ε^s [53]. To study the effects at far detector of DUNE, the coherent states $|\nu^s\rangle$ and $|\nu^d\rangle$ have to be used. We could also define a coherent state of $(\mathscr{M}_1|\nu_\mu\rangle + \mathscr{M}_2|\bar{\nu}_\tau\rangle)/\sqrt{|\mathscr{M}_1|^2 + |\mathscr{M}_2|^2}$ to describe the effects of the model in Sect. 2.2 but since no interference between evolved $|\nu_\mu\rangle$ and $|\bar{\nu}_\tau\rangle$ takes place even for long baselines, there is no point in introducing such a coherent state.

3 Spectrum of τ produced at forward experiments

In this section, we compute the spectrum of τ produced via different types of interaction introduced in this paper and

compare with the tau spectrum produced via the standard CC electroweak interactions.

The G_e coupling defined in Eq. (12) leads to

$$\langle |\mathcal{M}[\nu_e(E_\nu) + d(x) \to \tau^-(E_\tau) + u]|^2 \rangle = \langle |\mathcal{M}[\nu_e(E_\nu)$$
$$+ \bar{u}(x) \to \tau^-(E_\tau) + \bar{d}]|^2 \rangle =$$
$$\langle |\mathcal{M}[\bar{\nu}_e(E_\nu) + \bar{d}(x) \to \tau^+(E_\tau) + \bar{u}]|^2 \rangle = \langle |\mathcal{M}[\bar{\nu}_e(E_\nu)$$
$$+ u(x) \to \tau^+(E_\tau) + d]|^2 \rangle =$$
$$2G_e^2 (P_\tau \cdot P_\nu)(P_u \cdot P_d) = 2G_e^2 x^2 m_N^2 (E_\nu - E_\tau)^2, \quad (16)$$

where $m_\tau^2/(2xm_N) < E_\tau < E_\nu$. Thus, the differential cross sections of all these four processes can be written as

$$\frac{d\sigma}{dE_\tau} = \frac{1}{16\pi}\frac{1}{E_\nu s}|\mathcal{M}|^2 = \frac{G_e^2}{16\pi} xm_N \left(1 - \frac{E_\tau}{E_\nu}\right)^2 \frac{m_\tau^2}{2xm_N}$$
$$< E_\tau < E_\nu. \quad (17)$$

We can then write

$$\sigma(\nu_e + \text{nucleus} \to \tau + X) = \frac{G_e^2}{48\pi} m_N E_\nu \int_{x_{min}}^1$$
$$x \left(1 - \frac{m_\tau^2}{2xm_N E_\nu}\right)^3 [F_d(x, t) + F_{\bar{u}}(x, t)]dx \quad (18)$$

$$\sigma(\bar{\nu}_e + \text{nucleus} \to \bar{\tau} + X) = \frac{G_e^2}{48\pi} m_N E_\nu \int_{x_{min}}^1$$
$$x \left(1 - \frac{m_\tau^2}{2xm_N E_\nu}\right)^3 [F_{\bar{d},t}(x, t) + F_u(x, t)]dx \quad (19)$$

where F_q is the q-quark parton distribution function and

$$x_{min} = \frac{m_\tau^2}{2m_N E_\nu} \quad \text{and} \quad t = 2xm_N(E_\tau - E_\nu).$$

The spectrum of $\tau + \bar{\tau}$ produced by $\nu_e + \text{nucleus} \to \tau + X$ and $\bar{\nu}_e + \text{nucleus} \to \bar{\tau} + X$ can be written as

and

$$\frac{d\sigma(\bar{\nu}_\tau + u \to \tau^+ + d)}{dE_\tau} = \frac{d\sigma(\nu_\tau + \bar{u} \to \tau^- + \bar{d})}{dE_\tau}$$
$$= \frac{2m_N x G_F^2}{\pi} \left(\frac{E_\tau}{E_\nu}\right)^2 \frac{m_W^4}{[2(E_\nu - E_\tau)xm_N + m_W^2]^2} \quad (22)$$

where

$$\frac{m_\tau^2}{2xm_N} < E_\tau < E_\nu.$$

Notice that while in Eq. (17), we have used the effective four-Fermi coupling, G_e, in Eqs. (21, 22), we have used the full propagator for W. This is understandable as for $x \sim 0.1$, $2xm_N E_\nu \lesssim m_W^2 \ll m_{\phi_1^+}^2, m_{\phi_2^+}^2$. In fact, we have found that neglecting $2(E_\nu - E_\tau)xm_N$ in the denominator induces an error of 3% in the total number of events.

The total cross section of ν_τ and $\bar{\nu}_\tau$ scattering off the nucleon within the SM can be written as

$$\frac{d\sigma_\nu^{SM}}{dE_\tau} = \int_{x_{min}}^1 [F_d(x, t)\frac{d\sigma(\nu_\tau + d \to \tau^- + u)}{dE_\tau}$$
$$+ F_{\bar{u}}(x, t)\frac{d\sigma(\nu_\tau + \bar{u} \to \tau^- + \bar{d})}{dE_\tau}]dx$$

and

$$\frac{d\sigma_{\bar{\nu}}^{SM}}{dE_\tau} = \int_{x_{min}}^1 [F_{\bar{d}}(x, t)\frac{d\sigma(\bar{\nu}_\tau + \bar{d} \to \tau^+ + \bar{u})}{dE_\tau}$$
$$+ F_u(x, t)\frac{d\sigma(\bar{\nu}_\tau + u \to \tau^+ + d)}{dE_\tau}]dx.$$

Finally we can write

$$\sigma_\nu^{SM} = \int_{x_{min}}^1 \int_{m_\tau^2/(2xm_N)}^{E_\nu} [F_d(x, t)\frac{d\sigma(\nu_\tau + d \to \tau^- + u)}{dE_\tau}$$
$$+ F_{\bar{u}}(x, t)\frac{d\sigma(\nu_\tau + \bar{u} \to \tau^- + \bar{d})}{dE_\tau}]dE_\tau dx$$

$$S_e(E_\tau) = \frac{\int_{E_\tau} \int_{x_{min}}^1 [F_{\nu_e}(E_\nu)(F_d + F_{\bar{u}}) + F_{\bar{\nu}_e}(E_\nu)(F_{\bar{d}} + F_u)]\frac{d\sigma}{dE_\tau} dE_\nu dx}{\int \int_{x_{min}}^1 \int_{m_\tau^2/(2xm_N)}^{E_\nu} [F_{\nu_e}(E_\nu)(F_d + F_{\bar{u}}) + F_{\bar{\nu}_e}(E_\nu)(F_{\bar{d}} + F_u)]\frac{d\sigma}{dE_\tau}dE_\tau \, dx \, dE_\nu}, \quad (20)$$

where $d\sigma/dE_\tau$ is given in Eq. (17). The parton distribution functions are functions of both x and the Mandelstam variable, t.

For comparison the standard model cross sections are

$$\frac{d\sigma(\nu_\tau + d \to \tau^- + u)}{dE_\tau} = \frac{d\sigma(\bar{\nu}_\tau + \bar{d} \to \tau^+ + \bar{u})}{dE_\tau}$$
$$= \frac{2m_N x G_F^2}{\pi} \frac{m_W^4}{[2(E_\nu - E_\tau)xm_N + m_W^2]^2} \quad (21)$$

and a similar formula for $\sigma_{\bar{\nu}}^{SM}$ replacing particles with antiparticles.

As discussed in Sect. 2.1, the effective $G_{\nu\mu}$ coupling introduced in Eq. (1) can also lead to the τ production via charged pion decay. The signal from $\pi^+ \to \mu^+ \nu_\tau$ and $\pi^- \to \mu^- \bar{\nu}_\tau$ will have the following form
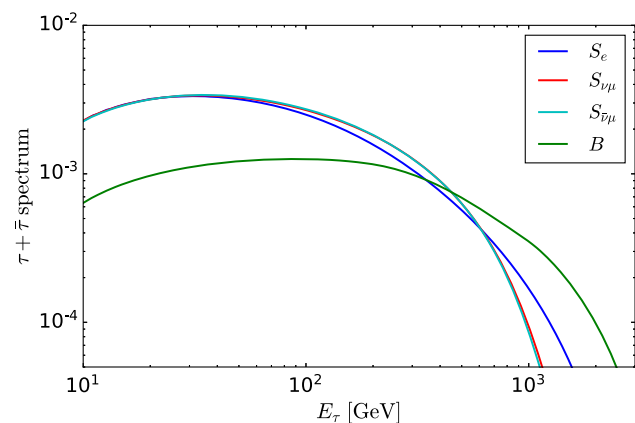
$$S_{\nu\mu}(E_\tau) \equiv \frac{\int_{E_\tau} [F_{\nu_\mu}^\pi(E_\nu)\frac{d\sigma_\nu^{SM}}{dE_\tau} + F_{\bar{\nu}_\mu}^\pi(E_\nu)\frac{d\sigma_{\bar{\nu}}^{SM}}{dE_\tau}]dE_\nu}{\int [F_{\nu_\mu}^\pi(E_\nu)\sigma_\nu^{SM} + F_{\bar{\nu}_\mu}^\pi(E_\nu)\sigma_{\bar{\nu}}^{SM}]dE_\nu}, \quad (23)$$

where $F_{\nu_\mu}^\pi(E_\nu)$ and $F_{\bar\nu_\mu}^\pi(E_\nu)$ are the spectra of neutrinos from the pion decay (rather than the whole flux from pion and Kaon decay).

Let us now discuss the spectrum of the tau produced by lepton number and lepton flavor violating pion decay mode caused by the effective coupling $G_{\bar\nu\mu}$ introduced in Eq. (9) of Sect. 2.3. The signal from $\pi^+ \to \mu^+ \bar\nu_\tau$ and $\pi^- \to \mu^- \nu_\tau$ will have a form given by Eq. (23), swapping F_{ν_μ} and $F_{\bar\nu_\mu}$:

$$S_{\bar\nu\mu}(E_\tau) \equiv \frac{\int_{E_\tau}[F_{\bar\nu_\mu}^\pi(E_\nu)\frac{d\sigma_\nu^{SM}}{dE_\tau} + F_{\nu_\mu}^\pi(E_\nu)\frac{d\sigma_{\bar\nu}^{SM}}{dE_\tau}]dE_\nu}{\int[F_{\bar\nu_\mu}^\pi(E_\nu)\sigma_\nu^{SM} + F_{\nu_\mu}^\pi(E_\nu)\sigma_{\bar\nu}^{SM}]dE_\nu}. \quad (24)$$

Finally the τ spectrum within the standard model will have the form

$$B = \frac{\int_{E_\tau}[F_{\nu_\tau}(E_\nu)\frac{d\sigma_\nu^{SM}}{dE_\tau} + F_{\bar\nu_\tau}(E_\nu)\frac{d\sigma_{\bar\nu}^{SM}}{dE_\tau}]dE_\nu}{\int[F_{\nu_\tau}(E_\nu)\sigma_\nu^{SM} + F_{\bar\nu_\tau}(E_\nu)\sigma_{\bar\nu}^{SM}]dE_\nu}. \quad (25)$$

From Eqs. (18, 19, 21, 22), we observe that the cross sections of all the processes are suppressed by x for small values of x. As a result, the main contribution to the cross section comes from $x \sim \text{few} \times 10^{-2} - 1$. Thus, $Q^2 = -t = 2(E_\nu - E_\tau)x m_N \sim 100\,\mathrm{GeV}^2$.

The normalized spectra of $\tau + \bar\tau$ from each scenario are shown in Fig. 1. To draw the curves, we have averaged the scattering cross section over the protons and neutrons composing Tungsten nucleus. As seen from the figure, the background from SM is significantly harder than new physics. This is mostly due to the fact that the background comes from $F(\nu_\tau)$ and $F(\bar\nu_\tau)$ which are harder than the spectra of other neutrino flavors; cf., Eq. (25) with Eqs. (20, 23, 24). The spectrum of background is quite distinct from $S_{\nu\mu}$ and

$S_{\bar\nu\mu}$ so as we shall see in the next section, using the information on spectra will considerably boost the sensitivity to the new physics. However, the spectra $S_{\nu\mu}$ and $S_{\bar\nu\mu}$ are very close to each other and cannot be distinguished. This is due to the fact that $F_{\nu_\mu}^\pi$ and $F_{\bar\nu_\mu}^\pi$ are almost equal to each other; see Eqs. (23, 24). If an excess of $\tau + \bar\tau$ is discovered, it will not be possible to distinguish if it comes from the lepton number conserving $\pi^+ \to \mu^+ \nu_\tau$ process or from the lepton number violating $\pi^+ \to \mu^+ \bar\nu_\tau$ process at FASERν by studying the energy spectrum of the events. One suggestion is to attune Q1-3 quadrupole and D1 dipole (located close to the interaction point) such that the transverse distribution of neutrinos emitted from π^+ and π^- decays can be distinguished from one another.

The uncertainties in the predictions of the fluxes of ν_μ, $\bar\nu_\mu$, ν_e and $\bar\nu_e$ are relatively small but the predictions for ν_τ and $\bar\nu_\tau$ suffer from large uncertainties. Ref. [11] shows that the different simulators predict the ν_τ flux which can differ from each other by more than 100%. To draw the $\tau + \bar\tau$ spectrum, we have used neutrino fluxes from a simulator whose prediction is close to the median of the predictions of other simulators and is therefore recommended by Ref. [11]. More details are described in the end of Sect. 4. We shall show in Sect. 5 that the number of events from new physics at FASERν will be too low to reconstruct the spectra but, at FASERν2 with about 400 times more statistics, reconstructing the spectra of the events from new physics may become possible. By then, more dedicated simulations can reduce uncertainties in the neutrino flux predictions. Moreover, as we discuss in the next section, the data from FASERν during the run III of the LHC can itself determine which simulator for the neutrino fluxes is valid. Thus, before the start of high luminosity run of the LHC and FASERν2 data taking, the uncertainty in the standard model prediction for the neutrino fluxes can be significantly reduced.

4 Characteristics of FASERν, SND@LHC and FASERν2

The FASERν and SND@LHC detectors are respectively located in the side tunnels TI12 and TI18, 480 m downstream the ATLAS Interaction Point (IP). FASERν is composed of 1000 emulsion layers interleaved with 1 mm tungsten plates [9]. The effective masses of FASERν [9] and SND@LHC [10] are respectively 1.2 ton and 800 kg and their sizes are 25 cm × 25 cm × 1.3 m and 41.6 cm × 38.7 cm × 32 cm, respectively. Both detectors boast having excellent spatial and angular resolution in reconstructing the tracks of charged particles which will enable them to resolve the ν_τ CC events. The details of the FASERν and SND@LHC detectors are presented in [9] and in [10], respectively. An updated prediction for the fluxes at these detectors can be found in [11].

Fig. 1 Spectra of $\tau + \bar\tau$ produced at FASERν normalized to 1. The curves marked with S_e, $S_{\nu\mu}$ and $S_{\bar\nu\mu}$ show the spectra of $\tau + \bar\tau$ from new physics scenarios $\nu_e + \text{nucleus} \to \tau + X$, $\pi^+ \to \mu^+\nu_\tau$, $\pi^+ \to \mu^+\bar\nu_\tau$, respectively. The standard model background is marked with B. The input neutrino spectra that we insert to draw the $\tau + \bar\tau$ spectrum (i.e., F_{ν_τ}, $F_{\bar\nu_\tau}$ $F_{\nu_\mu}^\pi$ and $F_{\bar\nu_\mu}^\pi$) are described in the last paragraph of Sect. 4

The upgrade of FASERν for the high luminosity LHC will have a size of 40 cm × 40 cm × 8 m and a mass of 20 tonnes [54]. The proposed location of this detector could be slightly off-axis at a distance of 620 meter or on-axis at a distance of 480 meter from the interaction point [54]. Ref. [11] has also predicted the neutrino within the SM at this detector which is assumed to be placed 620 m downstream from the ATLAS IP.[6]

According to [41], the efficiency of FASERν in detecting 1-prong τ decay is 75% and that of 3-prong decay is 15%. Considering that the branching ratios of 1-prong and 3-prong are respectively 85% and 15%, we take the average efficiency of 67% for the ν_τ detection at FASERν. We take similar efficiency for the tau neutrino detection at SND@LHC. Considering table II of [9], throughout our analysis, unless it is stated otherwise, we take 15% uncertainty in the neutrino flux normalization.

It is shown in Ref. [9] that the resolution of the ν_μ energy measurement will be 30%. However, to our best knowledge, similar analysis has not been carried out for the energy resolution of ν_τ and ν_e or for the detected τ. The tau particles at forward experiments will travel a distance of $L_{tr} \sim 1$ cm$(E_\tau/200$ GeV$)$ before decay. The direction of the momentum of τ (or equivalently, the direction of the line connecting decay and production vertices) can be reconstructed with a precision of $0.06(1$ cm$/L_{tr})$ mrad [4]. Due to the lepton flavor conservation, all decay modes of τ contain ν_τ which appears as missing energy momentum. In hadronic decay modes of τ, which constitute 65% of the decays, only one neutrino is emitted. By measuring the energy-momentums of visible particles and reconstructing the direction of τ momentum and using energy-momentum conservation, it will be therefore possible to reconstruct the τ energy for the hadronic decay modes. For example, in case of $\tau^+ \to \pi^+ \nu_\tau$, the energy of the final pion and the angle that it makes with the direction of the tau momentum determine the energy of the τ. Thanks to the sub-milliradian angular resolution of FASERν, the tiny angle $[O(10^{-2})]$ between the directions of tau and pion momenta can be measured with remarkable accuracy so the energy resolution in determining the tau energy will mainly be limited by the energy resolution in measuring the energy of π^+. We take nominal value of 30% for the τ energy reconstruction when necessary. As we shall see in the next session, at FASERν and SND@LHC during the run III of the LHC, the maximum signal events will be too small to justify binning the data so we shall only analyze the total number of predicted τ events for the run III in studying the sensitivity for new physics. We have examined the dependence of the results on the energy resolution. As expected in the case of no binning, the results appear to be independent of the resolution of the energy measurement.

As is well-known, the predictions of different simulators for the ν_τ and $\bar{\nu}_\tau$ spectra at the forward experiments are significantly different. The prediction of simulator, J for the number of τ events at the ith bin can be written as

$$
\begin{aligned}
B_i^J = \varepsilon_\tau N_W \int_{E_{min}^i}^{E_{max}^i} \int_{m_\tau} \int_{E_\tau} & \left[F_{\nu_\tau}^J (E_\nu) \frac{d\sigma_{CC}}{dE_\tau} \right. \\
& \times (\nu_\tau + \text{nucleus} \to \tau + X) \\
& + F_{\bar{\nu}_\tau}^J (E_\nu) \frac{d\sigma_{CC}}{dE_\tau} (\bar{\nu}_\tau + \text{nucleus} \to \tau^+ + X) \right] \\
& \times f(E_\tau', E_\tau) dE_\nu dE_\tau dE_\tau',
\end{aligned} \tag{26}
$$

where $F_{\nu_\tau}^J$ and $F_{\bar{\nu}_\tau}^J$ are respectively ν_τ and $\bar{\nu}_\tau$ energy spectra predicted by different simulators in Ref. [11]. The superscript J determines the simulator. $\varepsilon_\tau = 0.67$ is the efficiency of the ν_τ detection at the detector. $f(E_\tau', E_\tau)$ is the energy resolution function which we take to be a Gaussian with a 30% width. (E_{min}^i, E_{max}^i) determine the limits of the ith energy bin. N_W is the number of tungsten nuclei inside the detector, $N_W = M_D/M_W$ where $M_W = 183m_p$ and $M_D = 1.2$ ton for run III detector. In Table 4, we show our prediction for the number of events in different energy bins at FASERν.

Taking the uncertainty on the flux normalization to be $\sigma_\eta = 15\%$, we have computed χ_{rel}^2 as defined below for each model, J, and minimized over the pull parameter, f:

$$
\chi_{rel}^2 = \sum_i \left[\frac{[(1+f)B_i^{true} - N_i^J]^2}{B_i^{true}} \right] + \frac{f^2}{\sigma_\eta^2}. \tag{27}
$$

In computing χ_{rel}^2 that is shown in last column of Table 4, we take B_i^{true} to be equal to the prediction of Pythia8 (Hard). Notice that since our bin sizes are large, the results should be robust against the value of the energy resolution. As seen in Table 4, the FASERν experiment can discriminate between different simulators predicting the ν_τ flux with high confidence level. We therefore assume a well-known shape of the fluxes predicted within the SM in making forecast for FASERν2. We shall however study the impact of the normalization uncertainty.

We may wonder whether in the presence of the τ excess from new physics, FASERν can still discriminate between the simulators. As we shall see in Table 5, the maximum tau excess from new physics at FASERν will be ~ 5. If the true flux is close to the DPMJET 3.2017 prediction (which predicts the highest τ background of 59 events), addition of the excess will make it even more distinct from the rest of simulators. The excess of 5 events is too small to compensate for the predicted difference between DPMJET 3.2017 with 59 background events and Pythia8 with 25 background events. However, the background plus signal for SIBYLL 2.3c may come close to the Pythia8 prediction. We have computed χ_{rel}^2 for SIBYLL 2.3c prediction for background plus events from $Br(\pi^+ \to \mu^+ \nu_\tau) = 2.4 \times 10^{-3}$ using the binning

---

[6] https://github.com/KlingFelix/FastNeutrinoFluxSimulation.

Table 4 The number of τ events within the SM at FASERν using the prediction of three different simulators [11]. The relative χ^2 minimized over normalization uncertainty of 15% is shown in the last column, assuming Pythia8 (Hard) as the true model

Simulator	Bin limits in GeV					χ^2_{rel}
	< 50	50–100	100–500	500–1000	> 1000	
Pythia8 (Hard)	0.9	1.8	8.1	9.7	4.8	0.0
DPMJET 3.2017	1.5	3.1	16.2	23.3	14.5	43.7
SIBYLL 2.3c	0.7	1.1	3.7	3.1	0.7	9.6

described in Table 4. The result is $\chi^2_{rel} = 6.2$. That is even in the presence of maximum excess from new physics, FASERν can discriminate between the simulators at better than 99% C.L.

Hereafter in this study, for computing the SM background for the $\tau + \bar{\tau}$ events, we take the predictions of Pythia8 (Hard) given in Ref. [11] for F_{ν_τ} and $F_{\bar{\nu}_\tau}$. The Pythia8 (Hard) prediction is close to the median of the predictions of the DPMJET 3.2017 and SIBYLL 2.3c simulators. The other input spectra that we require for our computations are the fluxes of ν_μ and $\bar{\nu}_\mu$ that are sourced by charged pion mesons, $F^\pi_{\nu_\mu}$ and $F^\pi_{\bar{\nu}_\mu}$. Fortunately, the differences between the predictions by different simulators for $F^\pi_{\nu_\mu}$ and $F^\pi_{\bar{\nu}_\mu}$ are negligible. For our computations, we use the average of the predictions given in Ref. [11].

5 Signatures of the models in forward experiments

In this section, we study how FASERν and SND@LHC during LHC run III can constrain the models introduced in Sect. 2. We compare the bounds with the results of [22] which has performed a similar analysis within the framework of effective field theory. We also compare our bounds with the existing bounds and the one to be derived by upcoming DUNE experiment [55]. We then show how FASERν2 can improve the existing bounds with or without reconstructing the energy spectrum of τ.

$A.\pi^+ \to \mu^+ \nu_\tau$

Similarly to Eq. (26), we compute the number of signal events per bin as follows

$$\mathcal{N}_s^i = \varepsilon_\tau N_W Br(\pi^+ \to \mu^+ \nu_\tau) \int_{E^i_{min}}^{E^i_{max}}$$
$$\times \int_{m_\tau} \int_{E_\tau} \Big[F^\pi_{\nu_\mu}(E_\nu) \frac{d\sigma_{CC}}{dE_\tau}(\nu_\tau + \text{nucleus} \to \tau + X)$$
$$+ F^\pi_{\bar{\nu}_\mu}(E_\nu) \frac{d\sigma_{CC}}{dE_\tau}(\bar{\nu}_\tau + \text{nucleus} \to \tau^+ + X) \Big]$$
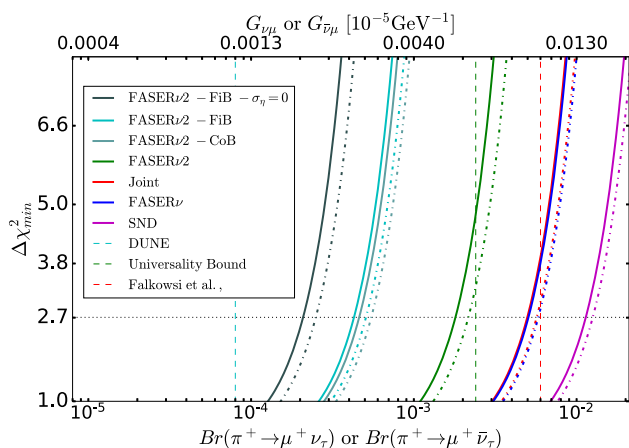$$\times f(E'_\tau, E_\tau) dE_\nu dE_\tau dE'_\tau \tag{28}$$

To compute the SM background per bin, B_i, we use Eq. (26). The total observed number in bin i is then $N_i^{obs} = B_i + \mathcal{N}_s^i$. We define the χ^2 as follows

$$\Delta\chi^2 = \sum_i \left[\frac{(B_i(1+\eta) - N_i^{obs})^2}{B_i} \right] + \frac{\eta^2}{\sigma_\eta^2} \tag{29}$$

where η is the pull parameter that takes care of the uncertainty in normalization, mainly coming from the uncertainty in the cross section and the flux normalization, $\sigma_\eta = 15\%$.

The second column in Table 5 shows total τ events ($\sum_i \mathcal{N}_s^i$) originated from $\pi^+ \to \nu_\tau \mu^+$ with a branching ratio saturating the present bound. As described in the end of Sect. 4, we take the median flux for ν_μ and $\bar{\nu}_\mu$ for our computation. We have examined using the hardest and softest predictions for ν_μ and $\bar{\nu}_\mu$ fluxes and have found a difference of about 5%, with total excess at FASERν varying between 4.56 to 5.04. Thus, the number of signal events at FASERν and SND@LHC during the run III of the LHC data cannot reach a statistical limit so for the purpose of searching for new physics, binning the data does not make sense. To compute

Table 5 Total expected number of τ events at FASERν and SND during the run III and at FASERν2 during the high luminosity run of the LHC. To compare the values, we have saturated the bounds on the new physics, setting G_e equal to 5×10^{-7} GeV^{-2} and the branching ratios to 2.4×10^{-3}. The last column shows the prediction for the SM background. The computation is made using the neutrino fluxes as described in the last paragraph of Sect. 4

Detector	$Br(\pi^+ \to \nu_\tau \mu^+)$	$Br(\pi^+ \to \bar{\nu}_\tau \mu^+)$	G_e	SM
SND@LHC	1.0	0.9	0.003	6.6
FASERν	4.9	4.3	0.027	25.3
FASERν2	1125.9	938.0	9.6	3403.3

Fig. 2 $\Delta\chi^2_{min}$ versus $Br(\pi^+ \rightarrow \mu^+\nu_\tau)$ (solid curves) or versus $Br(\pi^+ \rightarrow \mu^+\bar{\nu}_\tau)$ (dash-dotted curves). Purple, blue and green curves respectively correspond to SND@LHC, FASERν and FASERν2 without binning. The red curve shows the $\Delta\chi^2_{min}$ for SND@LHC and FASERν combined. The curves marked with "FiB" and "CoB" show $\Delta\chi^2_{min}$ for FASERν2 with an energy resolution of 30% and with two different binning patterns corresponding to fine and coarse binning. More detail are described in the text. Drawing all these curves, except the black one(s), we have assumed a 15% uncertainty in the normalization of the flux and have minimized over the corresponding pull parameter. Drawing the black curve(s), we have assumed zero uncertainty in the flux normalization and fine binning. The vertical lines from left to right correspond to the expected DUNE bound [55], the present bound from the lepton flavor universality constraint [27] and the forecast by [22] for FASERν, all at 90% C.L

χ^2 for these experiments, we consider only one bin (i.e., the total events). However, at FASERν2 during the high luminosity run the statistics will be large enough to use binning.

The solid lines in Fig. 2 show the χ^2 minimalized over η (the normalization uncertainty). For the solid curves, the horizontal axis is $Br(\pi^+ \rightarrow \mu^+\nu_\tau)$ which in terms of $G_{\nu\mu}$ can be written as $Br(\pi^+ \rightarrow \mu^+\nu_\tau) = (G_{\nu\mu}^2/8G_F^2)[m_\pi^4/(m_\mu^2(m_u + m_d)^2)]$. The upper horizontal axis shows the corresponding effective coupling. The purple, blue and red curves show χ^2 minimized over the flux normalization uncertainty for SND@LHC, FASERν and their combination, respectively. Since the normalization uncertainty mainly originates from the production rate at the interaction point which is common for SND@LHC and FASERν, we treat the uncertainty with a single pull parameter when combining the SND@LHC and FASERν predictions. That is for the joint analysis, we also use the definition of $\Delta\chi^2$ in Eq. (29) with i running over SND@LHC and FASERν experiments. For FASERν2, we have used three different binning schemes: (1) no binning; (2) coarse binning with bins divided as $E_\tau < 50$ GeV, 50 GeV $< E_\tau < 100$ GeV, 100 GeV $< E_\tau < 500$ GeV, 500 GeV $< E_\tau < 1$ TeV and 1 TeV $< E_\tau$; (3) fine binning with three bins at each energy decade. Drawing all these curves, we have taken an energy resolution of 30% in the E_τ determination. Of course, for no binning case, the results

do not depend on the energy resolution. Even for the coarse binning, χ^2 is robust against varying the energy resolution. In all curves, except for the black one(s), we have taken the flux normalization uncertainty equal to 15%. Comparing the FASERν2 curves with each other, it is clear that binning the data (or in other words, using the spectral information) dramatically increases the sensitivity to the new physics signal from $\pi^+ \rightarrow \mu^+ \overset{(-)}{\nu}_\tau$. Studying Fig. 1, this is understandable as the spectral shape of the background is considerably harder than the signal spectrum so the new physics signal cannot be hidden in the normalization uncertainty once the spectral uncertainty has been taken into account. Comparing black curve(s) with the rest, we observe that the uncertainty in the normalization significantly reduces the sensitivity.

Notice that for computing χ^2, we have set the "observed" number of events per bin equal to the "average" background plus the "average" predicted signal for "true" $Br(\pi^+ \rightarrow \mu^+ \overset{(-)}{\nu}_\tau)$ rather than having real data. Thus, if we want to minimize χ^2 over the only free parameter of the model which is $Br(\pi^+ \rightarrow \mu^+ \overset{(-)}{\nu}_\tau)$ we will invariably obtain zero. In fact, the χ^2 that we are computing will have a χ^2 distribution with only 1 (=number of pull parameters) degrees of freedom. As a results, regardless of the number of bins, the horizontal line at 2.7 represents 90% C.L. For example, we find that FASERν2 with coarse binning can constrain $Br(\pi^+ \rightarrow \mu^+\nu_\tau) < 4.6 \times 10^{-4}$ at 90% C.L.

The vertical line at 6×10^{-3} is the forecast at 90% for FASERν found by [22] which is in qualitative agreement with our results.[7] The vertical line at 2.4×10^{-3} shows the present bound from the flavor universality of π^+ decay [27]. Finally the forecast for DUNE near detector sensitivity at 90% is shown as a vertical line at 8×10^{-5} [55]. As seen from the figure, FASERν and SND@LHC will not be able to improve the present bounds but FASERν2 will have a good prospect of improving the bound or find a signal. Reconstructing the energy spectrum of τ with a moderate energy resolution can dramatically improve the reach for new physics.

We have also studied the robustness of the results against varying the flux prediction uncertainty. We have found that increasing the total flux uncertainty from 15 to 50%, the FASERν2 bound on $Br(\pi^+ \rightarrow \mu^+\nu_\tau)$ at 90% C.L. shifts from 1.8×10^{-3} to 6×10^{-3}. Moreover, we examine the possibility of 25% and 50% uncertainties in the flux shape by assigning different nuisance parameters for each bin. To be precise, we redefine $\Delta\chi^2$ as

$$\Delta\chi^2 = \sum_i \left[\frac{(B_i(1 + \eta_i) - N_i^{obs})^2}{B_i} + \frac{\eta_i^2}{\sigma_\eta^2} \right]$$

---

[7] In the notation of [22], $G_{\nu\mu} = 2(V_{CKM})_{11}(\epsilon_P)_{\mu\tau}/v^2$.

and we take σ_η equal to 0.25 and 0.5. η_i are the nuisance parameters for each bin over which we minimize $\Delta\chi^2$. Understandably, by introducing the flux shape uncertainty, the sensitivity decreases. For example, the 90% C.L. bound by FASERν2 coarse binning at 4.6×10^{-4} shifts to 2×10^{-3} with $\sigma_\eta = 0.25$ and to 4×10^{-3} with $\sigma_\eta = 0.5$. However, considering the advances to be made in the flux prediction by the time that FASERν2 starts data taking, it seems to be safe to take uncertainties well below 50% as we have done in drawing Fig. 2.

The effects appearing for $\pi^+ \to \nu_\tau \mu^+$ can be reinterpreted for a variety of other models, too. For example, let us consider a model that leads to the decay of π^+ to μ^+ and a sterile neutrino ν_s: $\pi^+ \to \mu^+ \nu_s$. As long as ν_s is lighter than ~ 1 MeV, the bound from flavor universality of the pion decay applies for this decay mode, too: $Br(\pi^+ \to \mu^+ \nu_s) < 2.4 \times 10^{-3}$. In principle, ν_s can have a mixing as large as $|U_{\tau 4}| \sim 0.3$ with ν_τ. Such scenario is motivated by the two anomalous ν_τ events observed by ANITA [56,57]. If the mass of ν_s is much smaller than 20 eV$(E_\nu/\text{TeV})^{1/2}(480$ m$/L)^{1/2}$, oscillation will not take place before reaching the FASERν detector so we would not have any excess due to $\nu_s \to \nu_\tau$. With a sterile neutrino mass of ~ 20 eV, there will be a τ excess with oscillatory behavior with E_ν. For sterile neutrino mass much larger than 20 eV, the $\nu_s \to \nu_e$ oscillation probability will average to $2|U_{\tau 4}|^2(1 - |U_{\tau 4}|^2)$ so there will be a τ excess with similar spectrum as that from $\pi^+ \to \nu_\tau \mu^+$. The discussion and results on $\pi^+ \to \nu_\tau \mu^+$ also applies for this case, replacing $Br(\pi^+ \to \nu_\tau \mu^+)$ with $2|U_{\tau 4}|^2(1-|U_{\tau 4}|^2)Br(\pi^+ \to \nu_s \mu^+)$. Notice that in the scenario described in this paragraph, unlike the canonical $3+1$ scheme, the sterile neutrino is produced by new physics (e.g., an intermediate new scalar) at pion decay rather than by oscillation. For a study of 3+1 scheme for the FASERν detector, see [58].

$B. \pi^+ \to \mu^+ \bar{\nu}_\tau$

The number of signal events in this case is given by Eq. (28) by replacing $Br(\pi^+ \to \mu^+ \nu_\tau)$ with $Br(\pi^+ \to \mu^+ \bar{\nu}_\tau)$ and swapping $F^\pi_{\bar{\nu}_\mu}(E_\nu)$ with $F^\pi_{\nu_\mu}(E_\nu)$ as follows

$$
\begin{aligned}
\mathcal{N}_s^i = \varepsilon_\tau N_W Br(\pi^+ \to \mu^+ \bar{\nu}_\tau) \int_{E_{min}^i}^{E_{max}^i} \int_{m_\tau} \int_{E_\tau} \\
\times \left[F^\pi_{\bar{\nu}_\mu}(E_\nu) \frac{d\sigma_{CC}}{dE_\tau}(\nu_\tau + \text{nucleus} \to \tau + X) \right. \\
\left. + F^\pi_{\nu_\mu}(E_\nu) \frac{d\sigma_{CC}}{dE_\tau}(\bar{\nu}_\tau + \text{nucleus} \to \tau^+ + X) \right] \\
\times f(E_\tau', E_\tau) dE_\nu dE_\tau dE_\tau',
\end{aligned}
\tag{30}
$$

The total number of signal events (summed over all bins) are shown in the third column of Table 5 for $Br(\pi^+ \to \mu^+ \bar{\nu}_\tau)$ saturating the bound from universality measurement

[27]. Similarly to the lepton number conserving case, the uncertainty in the signal prediction induced by the ν_μ and $\bar{\nu}_\mu$ flux uncertainties is only 5%. The corresponding χ^2 is also shown in Fig. 2 with dash-dotted line. The bound at 2.4×10^{-3} from the flavor universality of the pion decay applies for this model, too. Since $F_{\nu_\mu} \simeq F_{\bar{\nu}_\mu}$, the curves corresponding to $Br(\pi^+ \to \mu^+ \nu_\tau)$ and $Br(\pi^+ \to \mu^+ \bar{\nu}_\tau)$ are very close to each other.

$C. \nu_e + \text{nucleus} \to \tau + X$

Let us now assess the effects of G_e and the $\nu_e + \text{nucleus} \to \tau + X$ process introduced in Sect. 2.3. The excess in τ events in this case can be written as

$$
\begin{aligned}
\mathcal{N}_s^i = \varepsilon_\tau N_W \int_{E_{min}^i}^{E_{max}^i} \int_{m_\tau} \int_{E_\tau} \left[F_{\nu_e}(E_\nu) \frac{d\sigma_{CC}}{dE_\tau} \right. \\
\times (\nu_e + \text{nucleus} \to \tau + X) \\
\left. + F_{\bar{\nu}_e}(E_\nu) \frac{d\sigma_{CC}}{dE_\tau}(\bar{\nu}_e + \text{nucleus} \to \tau^+ + X) \right] \\
\times f(E_\tau', E_\tau) dE_\nu dE_\tau dE_\tau',
\end{aligned}
\tag{31}
$$

Equating G_e with the bound from $\tau^- \to \pi^- \nu_e$ (i.e., setting $G_e = 5 \times 10^{-7}$ GeV^{-2}), Table 5 shows the predicted number of events at FASERν, SND@LHC and FASERν2. Even at FASERν2, the number of the signal events cannot exceed 10. The values displayed in Table 5 correspond to the median ν_e and $\bar{\nu}_e$ fluxes as described in the end of Sect. 4. Taking the hardest flux in [11] the signal prediction increases only by 25%. As a result, we confirm the conclusion of [22] that the planned forward experiments cannot improve the bounds on G_e.

6 Summary and discussion

We have shown that the FASERν detector will provide a breakthrough on our understanding of the interactions of the third generation leptons. We have focused on three beyond SM LFV processes that can give rise to a τ excess at the FASERν detector: (i) $\pi^+ \to \mu^+ \nu_\tau$, (ii) $\pi^+ \to \mu^+ \bar{\nu}_\tau$ and (iii) $\nu_e + \text{nucleus} \to \tau + X$. We have introduced three models based on adding new scalars charged under electroweak symmetry that give rise to these processes. We have shown that by imposing proper global $U(1)$ flavor symmetries, the desired flavor patterns of the Yukawa couplings between the SM fermions can be explained. The same symmetry can also explain the smallness of the masses of the first generation fermions of the SM.

Our model for $\pi^+ \to \mu^+ \nu_\tau$ contains two new scalar doublets coupled respectively to the leptons and the quarks. In the presence of a mixing between the charged components of the two doublets, integrating out the heavy intermediate states we obtain a pseudoscalar–scalar four Fermi

effective coupling, $G_{\nu\mu}$, shown in Eq. (1) which gives rise to $\pi^+ \to \mu^+ \nu_\tau$ with a rate enhanced by $m_\pi^2/(m_u + m_d)^2$. The bound on the deviation of $\Gamma(\pi^+ \to e^+ \nu)/\Gamma(\pi^+ \to \mu^+ \nu)$ from the standard model prediction [27] then implies $G_{\nu\mu} < 4 \times 10^{-8}$ GeV^{-2}. The $G_{\nu\mu}$ coupling can also lead to $\nu_\tau + \text{nucleus} \to \mu^+ + X$ in the neutrino scattering experiments but without the $m_\pi^2/(m_u + m_d)^2$ enhancement. The bound on $G_{\nu\mu}$ renders this effect negligible while having $Br(\pi^+ \to \nu_\tau \mu^+) \sim 10^{-3}$ which can lead to a sizable τ excess in the forward experiments. We have shown that in terms of the formalism developed to study the effects of charged current non-standard interaction on neutrino experiments, we can write $\varepsilon_{\mu\tau}^s = [Br(\pi^+ \to \nu_\tau \mu^+)]^{1/2}$ so thanks to the $m_\pi^2/(m_u + m_d)^2$ enhancement, $\varepsilon_{\mu\tau}^s$ can be as large as $O(\text{few} \times 10^{-2})$. We have argued that bounds from NOMAD on the τ production do not constrain this model because the energy of the neutrino flux produced by the pion (rather than the Kaon) decay in the NOMAD experiment is too low to lead to the τ production. In our model, the bounds from $\tau^+ \to \mu^+ \pi^0$ can be satisfied because the neutral components of the new scalar doublets do not mix. We have pointed out that the model can also explain the observed $(g-2)_\mu$ deviation from the SM prediction.

By changing the flavor $U(1)$ charge assignment to the leptons in the model described above, we obtain a model giving rise to the G_e effective coupling in Eq. (12) which leads to $\nu_e + \text{nucleus} \to \tau + X$. The G_e coupling yields LFV decay mode $\tau^+ \to \pi^+ \nu$ with a rate enhanced by $m_\pi^2/(m_u + m_d)^2$. The strong bound on this decay mode severely constrains G_e. The model for the lepton number violating $\pi^+ \to \mu^+ \bar{\nu}_\tau$ is based on introducing a scalar doublet coupled to the quarks plus a singlet charged scalar with an off-diagonal coupling to left-handed doublets of the second and third generations. Such a singlet is also motivated with a small anomaly observed in the τ decay [26,43]. We find that in the same range of the parameter space that can explain this deviation from the SM prediction, a sizable rate of $\pi^- \to \mu^- \nu_\tau$ (leading to discernible tau excess in the forward experiments) can be obtained.

The bounds on the effective coupling discussed from the (lepton+ missing energy) signal at the LHC [22,59] do not apply for our models because the new intermediate states whose integrating out lead to these effective couplings have mass around $O(300 \text{ GeV})$ which is close to the center of mass energy of the partons scattering at the LHC. That is at the LHC, we cannot use the effective coupling formalism to describe the effects of new physics described in the present paper. We have briefly discussed the production of the new scalars and their potential signals at CMS and ATLAS [60, 61].

We have then studied the potential of forward experiments to test these models by looking for the τ event excess. The bound forecasts for FASERν and SND@LHC by the present work is in agreement with those found in Ref. [22]. We have proceeded by studying the energy spectrum of the tau events and showed that since the energy spectrum of the signal is going to be considerably softer than the τ event background, constructing the energy spectrum at FASERν2 can significantly improve the sensitivity to the new physics. We have discussed the possible resolution of the τ energy reconstruction at FASERν2 and demonstrated the dependence of sensitivity to the new physics signal on the energy binning scheme.

References

1. DONUT Collaboration, Observation of tau neutrino interactions, Phys. Lett. B **504**, 218 (2001). arXiv:hep-ex/0012035
2. DONuT Collaboration, Final tau-neutrino results from the DONuT experiment. Phys. Rev. D **78**, 052002 (2008). arXiv:0711.0728
3. OPERA Collaboration, Final results of the OPERA experiment on ν_τ appearance in the CNGS neutrino beam. Phys. Rev. Lett. **120**, 211801 (2018). arXiv:1804.04912
4. IceCube Collaboration, Measurement of astrophysical tau neutrinos in IceCube's high-energy starting events. arXiv:2011.03561
5. Super-Kamiokande Collaboration, Measurement of the tau neutrino cross section in atmospheric neutrino oscillations with Super-Kamiokande. Phys. Rev. D **98**, 052006 (2018). arXiv:1711.09436
6. P.B. Denton, Tau neutrino identification in atmospheric neutrino oscillations without particle identification or unitarity. Phys. Rev. D **104**, 113003 (2021). arXiv:2109.14576

7. IceCube Collaboration, Measurement of atmospheric tau neutrino appearance with IceCube DeepCore. Phys. Rev. D **99**, 032007 (2019). arXiv:1901.05366

8. T. Stanev, Possible tau appearance experiment with atmospheric neutrinos. Phys. Rev. Lett. **83**, 5427 (1999). arXiv:astro-ph/9907018

9. FASER Collaboration, Detecting and studying high-energy collider neutrinos with FASER at the LHC. Eur. Phys. J. C **80**, 61 (2020). arXiv:1908.02310

10. SHiP Collaboration, SND@LHC. arXiv:2002.08722

11. F. Kling, L.J. Nevay, Forward neutrino fluxes at the LHC. Phys. Rev. D **104**, 113008 (2021). arXiv:2105.08270

12. P. Bakhti, Y. Farzan, S. Pascoli, Unravelling the richness of dark sector by FASERν. JHEP **10**, 008 (2020). arXiv:2006.05437

13. B. Batell, J.L. Feng, S. Trojanowski, Detecting dark matter with far-forward emulsion and liquid argon detectors at the LHC. Phys. Rev. D **103**, 075023 (2021). arXiv:2101.10338

14. A. Ismail, R. Mammen Abraham, F. Kling, Neutral current neutrino interactions at FASERν. Phys. Rev. D **103**, 056014 (2021). arXiv:2012.10500

15. V.A. Mitsou, MoEDAL, FASER and future experiments targeting dark sector and long-lived particles. PoS **LHCP2020**, 112 (2021)

16. C.A. Argüelles et al., New opportunities at the next-generation neutrino experiments I: BSM neutrino physics and dark matter. Rept. Prog. Phys. **83**, 124201 (2020). arXiv:1907.08311

17. S. Ansarifard, Y. Farzan, Neutral Exotica at FASERν and SND@LHC. arXiv:2109.13962

18. P. Bakhti, Y. Farzan, S. Pascoli, Discovery potential of FASERν with contained vertex and through-going events. JHEP **04**, 075 (2021). arXiv:2010.16312

19. F. Kling, Probing light gauge bosons in tau neutrino experiments. Phys. Rev. D **102**, 015007 (2020). arXiv:2005.03594

20. B. Batell, J.L. Feng, M. Fieg, A. Ismail, F. Kling, R.M. Abraham et al., Hadrophilic dark sectors at the forward physics facility. arXiv:2111.10343

21. K.J. Kelly, F. Kling, D. Tuckler, Y. Zhang, Probing neutrino-portal dark matter at the forward physics facility. arXiv:2111.05868

22. A. Falkowski, M. González-Alonso, J. Kopp, Y. Soreq, Z. Tabrizi, EFT at FASERν. JHEP **10**, 086 (2021). arXiv:2105.12136

23. K. Jodłowski, S. Trojanowski, Neutrino beam-dump experiment with FASER at the LHC. JHEP **05**, 191 (2021). arXiv:2011.04751

24. M. Bahraminasr, P. Bakhti, M. Rajaee, Sensitivities to secret neutrino interaction at FASERν. arXiv:2003.09985

25. N. Beni et al., Further studies on the physics potential of an experiment using LHC neutrinos. J. Phys. G **47**, 125004 (2020). arXiv:2004.07828

26. A. Crivellin, F. Kirk, C.A. Manzari, L. Panizzi, Searching for lepton flavor universality violation and collider signals from a singly charged scalar singlet. Phys. Rev. D **103**, 073002 (2021). arXiv:2012.09845

27. PiENu Collaboration, Improved measurement of the $\pi \rightarrow$ eν branching ratio. Phys. Rev. Lett. **115**, 071801 (2015). arXiv:1506.05845

28. Particle Data Group Collaboration, Review of particle physics. PTEP **2020**, 083C01 (2020)

29. B.D. Sáez, K. Ghorbani, Singlet scalars as dark matter and the muon (g-2) anomaly. Phys. Lett. B **823**, 136750 (2021). arXiv:2107.08945

30. G. Hiller, C. Hormigos-Feliu, D.F. Litim, T. Steudtner, Anomalous magnetic moments from asymptotic safety. Phys. Rev. D **102**, 071901 (2020). arXiv:1910.14062

31. G. Hiller, C. Hormigos-Feliu, D.F. Litim, T. Steudtner, Model building from asymptotic safety with Higgs and flavor portals. Phys. Rev. D **102**, 095023 (2020). arXiv:2008.08606

32. H. Davoudiasl, W.J. Marciano, Tale of two anomalies. Phys. Rev. D **98**, 075011 (2018). arXiv:1806.10252

33. Muon g-2 Collaboration, Final report of the muon E821 anomalous magnetic moment measurement at BNL. Phys. Rev. D **73**, 072003 (2006). arXiv:hep-ex/0602035

34. Muon g-2 Collaboration, Measurement of the positive muon anomalous magnetic moment to 0.46 ppm. Phys. Rev. Lett. **126**, 141801 (2021). arXiv:2104.03281

35. T. Aoyama et al., The anomalous magnetic moment of the muon in the Standard Model. Phys. Rep. **887**, 1 (2020). arXiv:2006.04822

36. M. Davier, A. Hoecker, B. Malaescu, Z. Zhang, A new evaluation of the hadronic vacuum polarisation contributions to the muon anomalous magnetic moment and to $\alpha(m_Z^2)$. Eur. Phys. J. C **80**, 241 (2020). arXiv:1908.00921

37. M. Davier, A. Hoecker, B. Malaescu, Z. Zhang, Reevaluation of the hadronic vacuum polarisation contributions to the Standard Model predictions of the muon $g - 2$ and $\alpha(m_Z^2)$ using newest hadronic cross-section data. Eur. Phys. J. C **77**, 827 (2017). arXiv:1706.09436

38. M. Davier, A. Hoecker, B. Malaescu, Z. Zhang, Reevaluation of the hadronic contributions to the muon g-2 and to alpha(MZ). Eur. Phys. J. C **71**, 1515 (2011). arXiv:1010.4180

39. L. Allwicher, P. Arnan, D. Barducci, M. Nardecchia, Perturbative unitarity constraints on generic Yukawa interactions. arXiv:2108.00013

40. J. Haller, A. Hoecker, R. Kogler, K. Mönig, T. Peiffer, J. Stelzer, Update of the global electroweak fit and constraints on two-Higgs-doublet models. Eur. Phys. J. C **78**, 675 (2018). arXiv:1803.01853

41. ATLAS Collaboration, Searches for lepton-flavour-violating decays of the Higgs boson in $\sqrt{s} = 13$ TeV pp collisions with the ATLAS detector. Phys. Lett. B **800**, 135069 (2020). arXiv:1907.06131

42. NOMAD Collaboration, Final NOMAD results on muon-neutrino $-->$ tau-neutrino and electron-neutrino $—>$ tau-neutrino oscillations including a new search for tau-neutrino appearance using hadronic tau decays. Nucl. Phys. B **611**, 3 (2001). arXiv:hep-ex/0106102

43. HFLAV Collaboration, Averages of b-hadron, c-hadron, and τ-lepton properties as of 2018. Eur. Phys. J. C **81**, 226 (2021). arXiv:1909.12524

44. P.R. Burchat, Decays of the Tau Lepton, other thesis, 2 (1986)

45. V.V. Braguta, A.I. Onishchenko, rho meson form-factors and QCD sum rules. Phys. Rev. D **70**, 033001 (2004). arXiv:hep-ph/0403258

46. Y. Farzan, M. Tortola, Neutrino oscillations and non-standard interactions. Front. Phys. **6**, 10 (2018). arXiv:1710.09360

47. Y. Farzan, A model for large non-standard interactions of neutrinos leading to the LMA-dark solution. Phys. Lett. B **748**, 311 (2015). arXiv:1505.06906

48. Y. Farzan, I.M. Shoemaker, Lepton flavor violating non-standard interactions via light mediators. JHEP **07**, 033 (2016). arXiv:1512.09147

49. Y. Farzan, J. Heeck, Neutrinophilic nonstandard interactions. Phys. Rev. D **94**, 053010 (2016). arXiv:1607.07616

50. Y. Farzan, Viable models for large non-standard neutrino interactions. In 18th International Workshop on Neutrino Factories and Future Neutrino Facilities Search, 12 (2016). arXiv:1612.04971

51. Y. Farzan, A model for lepton flavor violating non-standard neutrino interactions. Phys. Lett. B **803**, 135349 (2020). arXiv:1912.09408

52. C. Biggio, M. Blennow, E. Fernandez-Martinez, General bounds on non-standard neutrino interactions. JHEP **08**, 090 (2009). arXiv:0907.0097

53. M. Blennow, S. Choubey, T. Ohlsson, D. Pramanik, S.K. Raut, A combined study of source, detector and matter non-standard neutrino interactions at DUNE. JHEP **08**, 090 (2016). arXiv:1606.08851

54. L.A. Anchordoqui et al., The forward physics facility: sites, experiments, and physics potential. arXiv:2109.10905

55. A. Giarnetti, D. Meloni, Probing source and detector nonstandard interaction parameters at the DUNE near detector. Phys. Rev. D **104**, 015027 (2021). arXiv:2005.10272

56. J.F. Cherry, I.M. Shoemaker, Sterile neutrino origin for the upward directed cosmic ray showers detected by ANITA. Phys. Rev. D **99**, 063016 (2019). arXiv:1802.01611

57. Y. Farzan, On the τ flavor of the cosmic neutrino flux. JHEP **07**, 174 (2021). arXiv:2105.03272

58. W. Bai, M. Diwan, M.V. Garzelli, Y.S. Jeong, M.H. Reno, Far-forward neutrinos at the large hadron collider. JHEP **06**, 032 (2020). arXiv:2002.03012

59. V. Cirigliano, A. Falkowski, M. González-Alonso, A. Rodríguez-Sánchez, Hadronic τ decays as new physics probes in the LHC era. Phys. Rev. Lett. **122**, 221801 (2019). arXiv:1809.01161

60. M. Hashemi, Observability of light charged Higgs decay to muon in top quark pair events at LHC. Eur. Phys. J. C **72**, 1994 (2012). arXiv:1109.5356

61. Y. Farzan, M. Hashemi, SLIM at LHC: LHC search power for a model linking dark matter and neutrino mass. JHEP **11**, 029 (2010). arXiv:1009.0829